Investigations on the Role of Proton-Coupled Electron Transfer in Hydrogen Activation by [FeFe]-Hydrogenase

ARTICLE *in* JOURNAL OF THE AMERICAN CHEMICAL SOCIETY · OCTOBER 2014

Impact Factor: 12.11 · DOI: 10.1021/ja508629m · Source: PubMed

7 AUTHORS, INCLUDING:

David Mulder
National Renewable Energy Laboratory
22 PUBLICATIONS **448** CITATIONS
SEE PROFILE

Maurizio Bruschi
Università degli Studi di Milano-Bicocca
79 PUBLICATIONS **1,862** CITATIONS
SEE PROFILE

Paul W King
National Renewable Energy Laboratory
58 PUBLICATIONS **2,085** CITATIONS
SEE PROFILE

JACS
JOURNAL OF THE AMERICAN CHEMICAL SOCIETY
Article
pubs.acs.org/JACS

Investigations on the Role of Proton-Coupled Electron Transfer in Hydrogen Activation by [FeFe]-Hydrogenase

David W. Mulder,[†] Michael W. Ratzloff,[†] Maurizio Bruschi,[‡] Claudio Greco,[‡] Evangeline Koonce,[§] John W. Peters,[§] and Paul W. King*[,†]

[†]Biosciences Center, National Renewable Energy Laboratory, Golden, Colorado 80401, United States
[‡]University of Milano-Bicocca, Department of Earth and Environmental Sciences, Piazza della Scienza 1, Milan, Italy
[§]Department of Chemistry and Biochemistry, Montana State University, Bozeman, Montana 59717, United States

Supporting Information

ABSTRACT: Proton-coupled electron transfer (PCET) is a fundamental process at the core of oxidation−reduction reactions for energy conversion. The [FeFe]-hydrogenases catalyze the reversible activation of molecular H_2 through a unique metallocofactor, the H-cluster, which is finely tuned by the surrounding protein environment to undergo fast PCET transitions. The correlation of electronic and structural transitions at the H-cluster with proton-transfer (PT) steps has not been well-resolved experimentally. Here, we explore how modification of the conserved PT network via a Cys → Ser substitution at position 169 proximal to the H-cluster of *Chlamydomonas reinhardtii* [FeFe]-hydrogenase (CrHydA1) affects the H-cluster using electron paramagnetic resonance (EPR) and Fourier transform infrared (FTIR) spectroscopy. Despite a substantial decrease in catalytic activity, the EPR and FTIR spectra reveal different H-cluster catalytic states under reducing and oxidizing conditions. Under H_2 or sodium dithionite reductive treatments, the EPR spectra show signals that are consistent with a reduced $[4Fe\text{-}4S]_H^+$ subcluster. The FTIR spectra showed upshifts of ν_{CO} modes to energies that are consistent with an increase in oxidation state of the $[2Fe]_H$ subcluster, which was corroborated by DFT analysis. In contrast to the case for wild-type CrHydA1, spectra associated with H_{red} and H_{sred} states are less populated in the Cys → Ser variant, demonstrating that the exchange of −SH with −OH alters how the H-cluster equilibrates among different reduced states of the catalytic cycle under steady-state conditions.

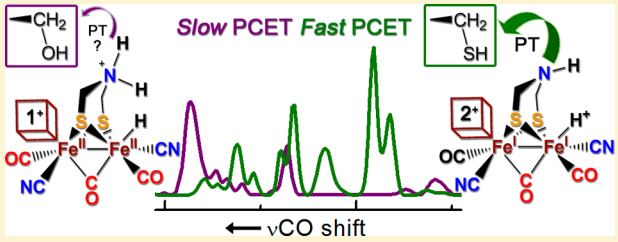

INTRODUCTION

Hydrogen (H_2) gas is an appealing energy carrier for the future, which has inspired efforts to develop biologically based approaches for renewable H_2 production.[1,2] The [NiFe]- and [FeFe]-hydrogenases are enzymes that catalyze the reversible activation of molecular H_2 through the reaction $H_2 \leftrightarrows 2H^+ + 2e^-$. Because hydrogenases accomplish this reaction near the thermodynamic potential of the H_2/H^+ couple[3] at high rates using base transition metals, the active sites of these enzymes and the mechanisms of H_2 activation provide models to help guide synthetic efforts.[4−9]

The catalytic site H-cluster of [FeFe]-hydrogenases consists of two subclusters, $[4Fe\text{-}4S]_H$ and $[2Fe]_H$, which are linked through a conserved cysteine (Cys) residue.[10,11] The $[2Fe]_H$ subcluster is ligated by strong-field CO and CN^- ligands along with a bridging azadithiolate (adt) ligand.[12,13] Altogether, the H-cluster is designed to carry out H_2 activation via proton-coupled electron transfer (PCET) reactions; the $[4Fe\text{-}4S]_H$ assists in electron relay[14−17] between either accessory FeS clusters (F-clusters) or external redox carriers[18] and adt functions to shuttle protons between proton-transfer (PT) networks and $[2Fe]_H$[13,19,20] during H_2 activation and proton reduction.[21−23] Details of proton transfer in the mechanism of H_2 activation by [FeFe]-hydrogenases have not been easily accessed experimentally or fully described. Thus, there is a need to closely examine how active site chemistry is functionally coupled to, and controls, the H-cluster electronic transitions during catalysis.

The importance of proton transfer (PT) for efficient H_2 activation has, in general, been shown by incorporation of proton relays in molecular catalysts that are a critical design component for improving catalytic performance.[24] PT pathways in [FeFe]-hydrogenases were initially identified from analysis of X-ray structures and have been tested by site-directed mutagenesis and chemical rescue.[10,11,25−30] The primary PT pathway consists of coordinated water molecules that form an H-bond network with conserved Glu and Ser residues, terminating at a strictly conserved Cys residue (Cys169 in CrHydA1). Cys169 is within H-bonding distance of the adt ligand of the H-cluster (Figure 1).[27] Computational models of the pathway dynamics show that PT involves final proton exchange between the Cys residue and the bridgehead amine.[31,32] Mutagenesis studies demonstrated that Cys169 is

Received: August 21, 2014
Published: October 6, 2014

   dx.doi.org/10.1021/ja508629m | J. Am. Chem. Soc. 2014, 136, 15394−15402

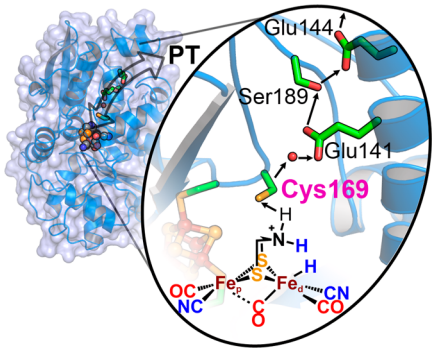

Figure 1. H-cluster and the conserved PT pathway in [FeFe]-hydrogenase. The numbering of amino acids is based on the sequence of CrHydA1. The structural cartoon and surface representations are from a homology model of CrHydA1 made from the H-cluster domain of *Clostridium pasteurianum* CpI (PDB ID 3C8Y).[33] Coloring scheme: carbon, green; oxygen, red; nitrogen, blue; sulfur, orange; iron, rust. The arrows depict the PT pathway.

critical for full catalytic activity, and exchange of −SH with either a more basic −OH (i.e., Ser) or nonpolar $-CH_3$ (i.e., Ala or Ile) residue led to severe reductions in both H_2 evolution and uptake activities.[27−30]

The effect of the substitution of Cys-to-Ser on the structural properties of the H-cluster was investigated in CrHydA1 (Cys169Ser) and *Clostridium pasteurianum* CpI (Cys299Ser).[28] Although the H-cluster was present and intact, the EPR and FTIR spectra[28] indicated it equilibrated into a H_{trans}-like state. The H_{trans} state was previously observed only in the [FeFe]-hydrogenase from *Desulfovibrio desulfuricans* (DdH) and is *transiently* formed during reductive activation (e.g., under H_2 or electrochemical reduction) of the oxidized inactive form of DdH.[34−40] The proposal that Cys169Ser equilibrated into H_{trans} was based on the Cys → Ser substitution affecting the H-cluster redox properties and/or H_2 binding in a similar manner.[28]

Here we examine the effects of a Cys169Ser substitution in CrHydA1 under steady-state conditions by EPR and FTIR spectroscopy and evaluate the electronic properties of this variant by complementary density functional theory (DFT) calculations. Our results show that spectral features assigned to different reduced states of wild-type (WT) CrHydA1[15−17,41] are observed in the Cys169Ser variant: however, at significantly altered intensities. Under reduction, Cys169Ser exhibited EPR spectra consistent with the presence of a $[4Fe\text{-}4S]_H^+$ subcluster[15] that strongly correlated with higher frequency ν_{CO} peaks in the accompanying FTIR spectra. DFT analysis of a Cys169Ser H-cluster model complex was used to calculate IR vibrational frequencies of CO/CN^- ligands and to help assign the oxidation state of $[2Fe]_H$. Isotope and exogenous CO binding effects on the spectroscopic signals were further explored to help characterize the nature of H-cluster intermediates.

EXPERIMENTAL METHODS

Expression and Purification. Site-directed mutagenesis of the Cys residue implicated in PT in both CrHydA1 (Cys169) and *Clostridium acetobutylicum* CaI (Cys298) were carried out using the XL site-directed mutagenesis kit (Stratagene) with pETDuet based plasmids described previously.[42,43] Plasmid constructs were confirmed by DNA sequencing before transformation into *Escherichia coli* NovaBlue (Novagen) for propagation. Expression and purification of Cys169Ser CrHydA1 and Cys298Ser CaI were carried out with slight modifications to a previously described procedure (Supporting Information).[43]

[FeFe]-Hydrogenase Sample Preparation. All samples were prepared in an MBraun glovebox under a nitrogen atmosphere and strict anaerobic conditions. H_2 treatments were carried out by 10 vacuum/flush cycles on a Schlenk link outfitted with an O_2 trap (Big O_2 Trap, Agilent Technologies, Inc., Santa Clara, CA, USA). For isotope studies, samples were exchanged into D_2O buffer using a G-25 column followed by incubation at 4 °C. Sparges with D_2 (99.7% D_2, Matheson Tri-Gas, Newark, CA USA) were carried out for 1 min followed by overnight incubation at 4 °C in the MBraun glovebox.

Spectroscopy. EPR and FTIR spectra were recorded on a ELEXSYS E500 CW spectrometer system (Bruker) and Nicolet 6700 FTIR spectrometer (Thermo Fisher Scientific), respectively. The resolution of the FTIR spectrometer was 2 cm^{-1}.

Computational Model of CrHydA1. The starting structure for the DFT calculations was based on the X-ray geometry of DdH (PDB ID 1HFe)[10] in which the water molecule bridging Fe_d and Fe_p was replaced by a CO group and the bridging propanedithiolate (pdt) ligand was replaced by adt.[12,13] The computational model, which is schematically shown in Figure S1 (Supporting Information), includes the bimetallic $[2Fe]_H$ cluster and selected residues of the second coordination sphere. A detailed description of this model is given in the Supporting Information. Calculations were carried out on models of WT CrHydA1 and the Cys169Ser variant, in which the −SH group of Cys169 was replaced with the −OH group of Ser.

DFT Calculations. Quantum mechanics (QM) calculations were carried out in the DFT framework with the TURBOMOLE suite of programs[44] by using the BP86 functional[45,46] in conjunction with the resolution-of-the-identity (RI) technique[47] and an all-electron valence triple-ζ basis set with polarization functions TZVP for all atoms.[48]

Vibrational analyses were carried out for all species in their minimum on the potential energy hypersurface using the same level of theory. Due to the atoms constrained at the original positions (see the Supporting Information), several very small negative eigenvalues of the Hessian were computed. However, these imaginary frequencies should not affect the (much higher in energy) ν_{CO} and ν_{CN} stretching modes. CO frequencies were scaled according to the scaling factor[49]

$$\nu_{CO}(\text{scal}) = 1.023\nu_{CO}(\text{cal}) - 49$$

Deuterium isotopic effects on the CO frequencies were investigated by replacing the hydrogen terminally coordinated to Fe_d with deuterium and recalculating vibrational frequencies from the Hessian. In some forms of the enzyme, an additional frequency was identified in the range of the CO and CN^- stretching frequencies. This frequency can be assigned to an N−H stretching mode of Lys228 associated with the hydrogen involved in the H-bond with Glu231. In fact, this N−H distance is unusually large and the corresponding NH- - -O_{Glu} distance unusually small, explaining the considerable shift to lower wavenumbers of this stretching mode, which is probably an artifact of the model used for the computational analysis. Since this mode can be coupled to the ν_{CO} and ν_{CN} stretching modes, thus possibly affecting their frequency values, we also replaced the H with D in order to shift the N−H stretching frequency well outside the region of the ν_{CO} and ν_{CN} stretching modes; notably, the additional set of calculations on such deuterated models did not yield any significant change in the computed ν_{CO} and ν_{CN} stretching frequencies, in comparison to the parent models.

RESULTS AND DISCUSSION

Biochemical Properties of Purified CrHydA1 Cys169Ser. The specific activity (U), defined as 1 μmol of H_2 produced min^{-1} mg^{-1}, ranged between 15 and 30 U for Cys169Ser CrHydA1. Although active, the level of H_2 evolution activity represents a significant decrease (30−50-fold) in comparison to WT CrHydA1 (748 U).[15] The use of increased concentrations of methyl viologen (MV, 80 mM) and NaDT (160 mM) resulted in increased H_2 evolution activity to a V_{max}

dx.doi.org/10.1021/ja508629m | J. Am. Chem. Soc. 2014, 136, 15394−15402

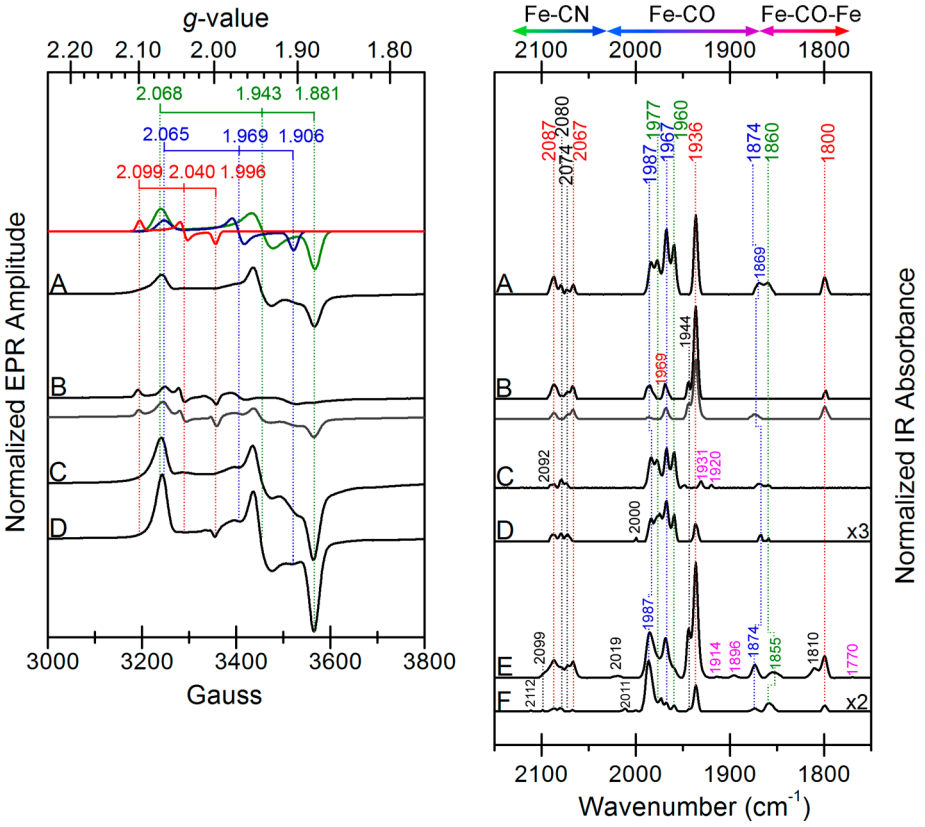

Figure 2. EPR and FTIR of Cys169Ser under steady-state reducing and oxidizing conditions (panels show EPR (left) and FTIR (right) spectra of Cys169Ser samples): (A) as isolated (20 mg/mL); (B) auto-oxidized sample 1 (dark shade, 12 mg/mL), sample 2 (light shade, 15 mg/mL); (C) NaDT (20 mg/mL); (D) 100% H_2 treated (15 mg/mL); (E) high-concentration as-isolated sample (120 mg/mL); (F) high-concentration 100% H_2 treated sample (120 mg/mL). Simulations of EPR signals (left panel) are shown at the top: red, rhombic 2.1 (H_{ox}); blue, rhombic 2.06; green, rhombic 2.07. The ν_{CN} and ν_{CO} peaks of FTIR spectra (right panel) correlating to rhombic 2.07, 2.06, and 2.1 signals are labeled in green, blue, and red, respectively. Peaks labeled in violet are similar to H_{red} and H_{sred} peaks determined from WT spectra.[15] FTIR spectra were collected at room temperature. EPR spectrometer settings: temperature, 11 K; microwave power, 1.0 mW; microwave frequency, 9.38−9.39 GHz; modulation frequency, 100 kHz; modulation amplitude, 10.0 G; time constant, 327.68 ms.

value of 84 U, further demonstrating that the Cys → Ser variant retains catalytic function, albeit at reduced levels. Despite the reduced activity, both EPR and FTIR spectra of Cys169Ser displayed strong spectroscopic signals, indicating that H-cluster incorporation was minimally affected during in vivo biosynthesis. This is consistent with the previous characterization of Cys169Ser CrHydA1;[28] however, those studies also reported that this variant was completely deficient in H_2 evolution and H_2 oxidation activities.

Spectroscopic Properties of As-Isolated Cys169Ser. We showed previously that, when WT CrHydA1 was purified in NaDT buffer, a major fraction equilibrated into the H_{ox} state, as observed by a strong rhombic 2.1 signal (g = 2.100, 2.039, 1.990), with minor contributions from reduced states.[15] In contrast, the EPR spectrum of an as-isolated sample of Cys169Ser prepared in buffer containing 5 mM NaDT primarily displayed two overlapping rhombic signals (rhombic 2.07, g = 2.068, 1.943, 1.881, T_{opt} = 11 K; rhombic 2.06, g = 2.065, 1.969, 1.906, T_{opt} = 23 K) and only a broad shoulder near g = 2.1, indicating a small contribution of H_{ox} (Figure 2A). Likewise, the FTIR spectrum displayed multiple peaks in the ν_{CO} (~1775−2030 cm^{-1}) and ν_{CN} stretching regions (~2030−2100 cm^{-1}) that are weaker in intensity in the WT spectrum.[15] Cys169Ser also showed weak signals for H_{ox}, H_{red}, and H_{sred} states (Figure 2A) that are stronger for WT CrHydA1 on the basis of our previous reports.[15]

Spectroscopic Properties of Oxidized Cys169Ser. The oxidation of as-isolated Cys169Ser was carried out by an auto-oxidization procedure, which involves exchange and equilibration into buffer without NaDT.[15] The resulting EPR spectra of oxidized Cys169Ser shown in Figure 2B yielded the appearance of a weak but well-resolved rhombic 2.1 signal (g = 2.099, 2.040, 1.996, T_{opt} = 20 K) of the H_{ox} state. The rhombic 2.06 EPR signal was also present at an intensity similar to that of the as-isolated sample (Figure 2A versus 2B), as determined by double-spin integration of the signal. The EPR spectra of the two oxidized Cys169Ser samples (Figure 2B) showed different levels of residual rhombic 2.07 signal, indicating different levels of conversion to the H_{ox} state. There was a minimal contribution of the CO inhibited state (H_{ox}-CO) to the spectra, which is indicative of H-cluster degradation. Further oxidation by methyl viologen gave an increase in signal intensity of the rhombic 2.1 signal along with the appearance of an axial g = 2.05 signal that can be assigned to H_{ox}-CO (Figure S4, Supporting Information). As also pointed out earlier,[28] the weak spectral intensity of auto-oxidized compared to as-isolated EPR spectra (20%, Figure 2B versus Figure 2A) is evidence for EPR-silent species formed upon auto-oxidation. In the earlier report,[28] no EPR signal was detected in the absence of NaDT. Two of the H-cluster states, H_{red} and H_{inact} (Figure 1), have been shown to be EPR silent.[34,35,39,41]

dx.doi.org/10.1021/ja508629m | J. Am. Chem. Soc. 2014, 136, 15394−15402

The FTIR spectrum of auto-oxidized Cys169Ser showed ν_{CO} peaks at 1800 cm^{-1} (μ-CO) and 1936 and 1969 cm^{-1} (terminal) and ν_{CN} peaks at 2067 and 2087 cm^{-1}, which are assigned to the H_{ox} state. Enrichment of the H_{ox} signal in the IR spectrum correlates nicely with the appearance of the EPR rhombic 2.1 signal assigned to H_{ox} (Figure 2B). Additional ν_{CO} peaks at 1944 and 1987 cm^{-1} indicate the presence of other intermediates. The peak at 1987 cm^{-1} mostly correlated with the presence of the rhombic 2.06 signal, and the peak at 1944 cm^{-1} more likely correlates to an EPR-silent species, since the latter peak has only been observed for oxidized samples.

Spectroscopic Properties of NaDT and H_2 Reduced CrHydA1 Cys169Ser. Reduction of oxidized Cys169Ser with excess NaDT (Figure 2C) primarily yielded the rhombic 2.07 signal, which was more sharp and intense than in the as-isolated Cys169Ser sample. Treatments with H_2 yielded similar spectra (Figure 2D), also primarily composed of the sharp rhombic 2.07 signal. This differed from the WT samples under H_2, which displayed a broadened signal (g = 2.3−2.07) in comparison to the rhombic 2.07 (Table S2, Supporting Information).[15] Also present in Cys169Ser under NaDT and H_2 reduction was a second, overlapping rhombic 2.06 signal, present at a intensity similar to that for the as-isolated and auto-oxidized samples. For the H_2 sample, the feature at g = 1.997 indicates a small presence of H_{ox} that likely did not react with H_2. Simulations show that the overall spectra of reduced samples consist of 86% of the 2.07 signal and 14% of the 2.06 signal. The power saturation dependency of the rhombic 2.07 signal was nearly identical with that of the WT rhombic 2.08 signal and saturated with increasing power at 11 K more quickly than at 23 K, indicating a similar source for the two signals (Figure S5, Supporting Information).

The source of the rhombic 2.07 signal in Cys169Ser is assigned to an S = 1/2 $[4Fe\text{-}4S]_H^+$ cluster and is highly related to the rhombic 2.08 signal observed in the WT CrHydA1.[15] The rhombic 2.06, however, has two possibilities: it originates from either a S = 1/2 $[2Fe\text{-}2S]^+$ (vide infra) on the basis of the temperature saturation (Figure S2)[15] or a S = 1/2 $[4Fe\text{-}4]_H^+$ that is similar to $[4Fe\text{-}4S]_H^+$ of the H_{trans} state.[34,35,39] The EPR signal assigned to H_{trans} shows g values (g = 2.06, 1.96, 1.89) and temperature properties ($[2Fe\text{-}2S]^+$-like) similar to those of the rhombic 2.06 of both WT[15] and Cys169Ser (Figure 2). For the H_{trans} signal, Mössbauer studies assigned the H-cluster oxidation state to $[4Fe\text{-}4S]_H^+$ paired with a diamagnetic $Fe^{II}Fe^{II}$ $[2Fe]_H$ subcluster.[37,38] An H_{trans} state was also reported for the as-isolated Cys169Ser by Knörzer et al.;[28] however, this assignment was based on an EPR signal with g values of 2.067, 1.941, and 1.880. Those g values more closely align with the g = 2.07 signal (2.068, 1.943, 1.881) we observed for Cys169Ser (Figure 2). They suggested that changes in redox properties could allow a nearby H_2O to react with Fe_d to produce a terminal −OH ligand as modeled by earlier DFT studies of H_{trans} and also H_{inact},[50,51] although this ligand has not yet been observed experimentally.[40] Thus, the two overlapping 2.07 and 2.06 EPR signals of Cys169Ser (and 2.08/2.06 for wild-type CrHydA1)[15] represent different states and are distinguished by slight differences in g tensor and temperature and power properties. We propose that these states arise from changes at $[2Fe]_H$ that lead to each state having a unique terminal ligand, electronic spin and charge distribution, coordination environment, and/or protonation state of adt.

The FTIR spectra of Cys169Ser reduced with NaDT (Figure 2C) or H_2 gas (Figure 2D) showed complexity in both the terminal ν_{CO} (1900−2030 cm^{-1}) and ν_{CN} (2030−2100 cm^{-1}) regions, with higher energy peak positions in comparison to WT CrHydA1. In addition, ν_{CO} peaks were observed in a region consistent with a "semibridging" (~1850−1880 cm^{-1}) or a bridging assignment but in a more oxidized $[2Fe]_H$ cluster. Small shifts for these peaks were observed between different samples, possibly reflecting the sensitivity of the "semi-bridging"/bridging ligand to dynamic Fe−H interactions, the protonation state of the adt ligand, and subtle changes in the H-cluster environment. Through analysis of spectral intensities, we assigned two sets of ν_{CO} peaks in reduced samples: set 1 with 1860, 1960, 1977 cm^{-1} and set 2 with 1874, 1967, 1987 cm^{-1}. Peaks of weaker intensity were also observed at 1920 and 1931 cm^{-1} and are assigned to the H_{red}/H_{sred} states.[15] The two sets of IR signals appear to correlate with the two EPR rhombic 2.07 (set 1) and 2.06 (set 2) signals. However, the potential for an EPR-silent species and the different temperatures for data collection between EPR (11−60 K) and FTIR (room temperature) prevent making a definitive assignment of these IR band sets to the EPR signals. Likewise, for more highly concentrated Cys169Ser samples treated with H_2 (Figure 2F), residual H_{ox} was observed as the presence of ν_{CO} peaks at 1800 and 1936 cm^{-1}. This may indicate a decreased ability of Cys169Ser to react with H_2 or incomplete H_2 treatment, which has also been observed to a lesser extent for H_2 treated WT CrHydA1.[15]

Observation of Hydrogen/Deuterium Isotope-Sensitive FTIR Peaks in Reduced Cys169Ser. A mechanism for H_2 activation by [FeFe]-hydrogenases has been proposed on the basis of crystallographic and FTIR analysis of reduced DdH and CrHydA1, whereby the μ-CO is proposed to alternate between bridging (H_{ox}) and terminal (H_{red}−H) orientations as the H-cluster transitions through a catalytic cycle.[10,16,20,40,41] This shift of μ-CO is assumed to occur along with formation of terminal H-ligands on $[2Fe]_H$.[50,52] It has been shown for metal−carbonyl organometallic complexes that terminal hydrides exert a strong trans influence on the trans ligand: in this case the μ-CO of $[2Fe]_H$. This can result in mixing of the ν_{FeH} with ν_{CO} modes and cause a hydrogen/deuterium isotope effect on the position of ν_{CO} in the IR spectrum.[53] Notably, the H/D isotope effect induces a shift of ν_{CO} to lower energies after H → D substitution, with only small to negligible effect on cis CO ligands.[54−56] Thus, reduction of [FeFe]-hydrogenases in H- or D-enriched buffers can be used to assign ν_{CO} peaks to the μ-CO ligand on the basis of an isotope induced shift and provide indirect evidence for an H species bound to the terminal position on $[2Fe]_H$.

As shown in Figure 3 (for detailed spectra, see Figure S6 in the Supporting Information), reduction of Cys169Ser by NaDT or H_2 produces ν_{CO} peaks in the 1860−1870 cm^{-1} region, which are consistent with a "semibridging"/bridging assignment. After exchange from H_2O → D_2O enriched buffers followed by reduction with NaDT or D_2, these peaks shifted to slightly lower energies. Specifically, the 1860 and 1868 cm^{-1} peaks shifted to 1853 and 1864 cm^{-1} after reduction with NaDT, and the peak observed at 1859 cm^{-1} under 100% H_2 treatment in H_2O shifted to 1853 cm^{-1} under 100% D_2 in D_2O buffer (Figure 3). These shifts are consistent with a change in mass of a terminal ligand on Fe_d that is positioned trans to the "semibridging" CO, supporting a terminal H species (e.g., hydride) coordinated to the Fe_d atom of $[2Fe]_H$ in these reduced states. The DFT calculations shown in Figure 3 on the reduced H-cluster in Cys169Ser simulated with either H or D

dx.doi.org/10.1021/ja508629m | J. Am. Chem. Soc. 2014, 136, 15394−15402

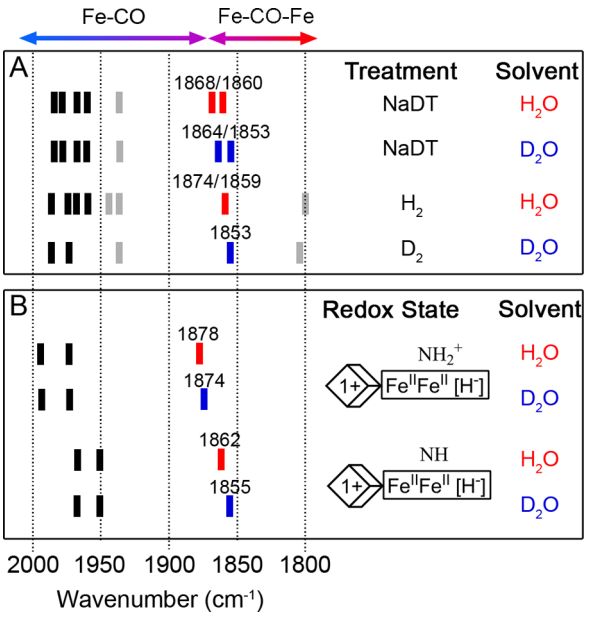

Figure 3. Comparison of experimental FTIR bands of reduced CrHydA1 Cys169Ser to calculated FTIR bands from a DFT model of Cys169Ser: (A) experimental FTIR bands in the ν_{CO} region from enzyme reduced with NaDT, H_2, or D_2 in buffer prepared with either H_2O or D_2O; (B) DFT calculated FTIR bands in the ν_{CO} region based on the Cys169Ser H-cluster model prepared in H_2O or D_2O solvent. Bands indicated in red (H_2O) are observed to shift to slightly lower energies under D_2O (blue). Bands in light gray are either assigned to the H_{ox} state or are unassigned.

terminal ligands also show a similar H → D induced downshift in the μ-CO peak.

DFT Calculations of the ν_{CO} Frequencies in Reduced Cys169Ser and WT Enzymes. The observation of the H → D exchange effect on the μ-CO bands called for a detailed DFT analysis of adducts featuring a terminal hydride trans to the μ-CO on Fe_d. In addition, a comparison of the FTIR spectrum of WT CrHydA1 to Cys169Ser after treatment with 100% H_2 shows that the principal ν_{CO} peaks shift to higher energies (Figure S7, Supporting Information), suggesting that binding H_2 to H_{ox} induces a further oxidation of the $[2Fe]_H$ subcluster from a mixed-valent $Fe^{II}Fe^{I}$ to a diferrous state. Notably, DFT vibrational analysis performed on Cys169Ser species, in which the $[2Fe]_H$ subcluster attains the $Fe^{II}Fe^{II}$ state and the $[4Fe\text{-}4S]_H$ cluster is modeled in the reduced $[4Fe\text{-}4S]_H^+$ state, shows that the principal ν_{CO} peaks occur at 1878, 1971, and 1992 cm^{-1} or 1862, 1951, and 1965 cm^{-1}, depending on the protonation state of the adt ligand (**3b** and **4b** in Figure 4 and Table 1). In particular, the assignments of ν_{CO} frequencies reported in Table 1 for **3b** and **4b** are associated with mean absolute errors (MAE) as low as 4 and 8 cm^{-1}, respectively, in comparison to the experimental frequencies. This suggests that these two experimentally assigned states might be distinguished by differences in the protonation state of the adt ligand. DFT calculations also show that in **3a,b** and **4a,b** a CO ligand is fully bridged between the two metal atoms.

Regarding the effects of H → D substitution on theoretical vibrational spectra, the exchange of an H- for a D-terminal ligand in the DFT models leads to a significant downshift in the μ-CO vibrational energies shown in Figure 3B and is in agreement with the experimental trends shown in Figure 3A. An analysis of the normal modes of vibration corresponding to

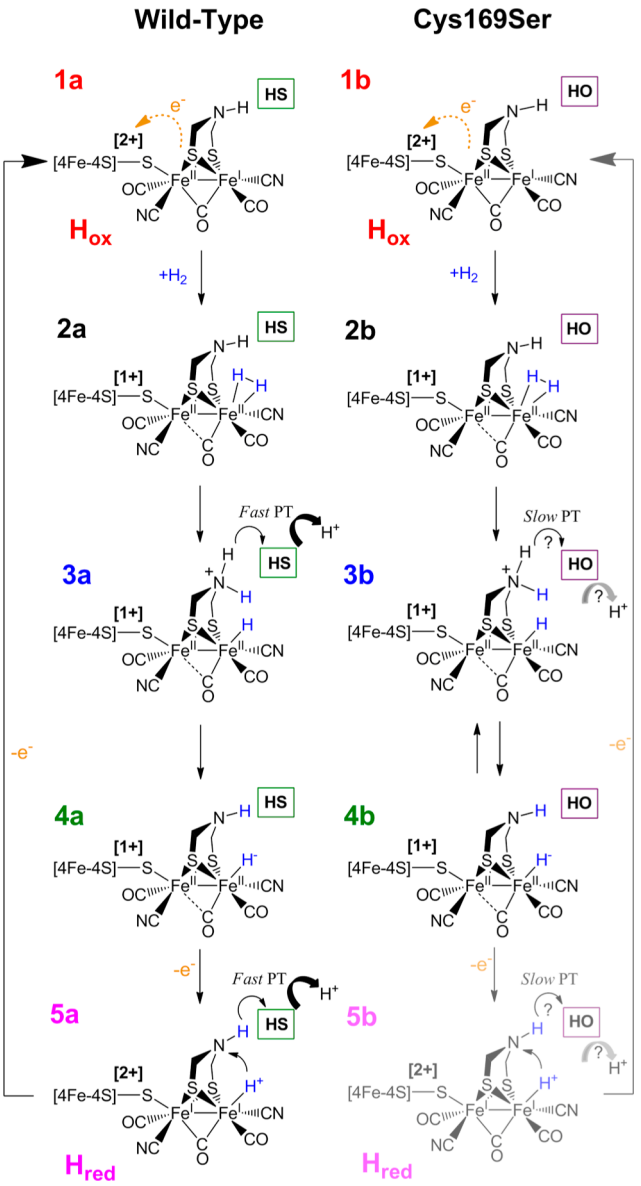

Figure 4. Proposed model for H_2 activation by WT and Cys169Ser variants of CrHydA1 based on experimental results and DFT calculations (Table 1). The respective thiol and hydroxyl side chains of nearby Cys and Ser residues are noted in green and purple boxes. DFT optimized geometries of H-cluster models **3a,b** and **4a,b** are shown in Figure S10 (Supporting Information).

the calculated 1878 and 1862 cm^{-1} frequencies in **3b** and **4b**, respectively, explains the effect of H → D replacement on the ν_{CO} frequencies. The stretching mode of the μ-CO trans to Fe−H/D is strongly coupled to the stretching of the Fe−H bond (Figure S9, Supporting Information). Indeed, H → D replacement leads to a downshift of the Fe−H stretching vibration by ~500 cm^{-1}, thus decoupling the μ-CO and Fe−H stretching modes in the deuterated species (Figure S9, Supporting Information).

A very good match between computed and experimental values was observed for WT CrHydA1 as well: in particular, a comparison between theoretical frequencies of model **4a** and the available experimental data highlights a MAE as low as 9 cm^{-1} (Table 1). The latter result suggests that the higher oxidation state intermediate also forms in WT CrHydA1. This

dx.doi.org/10.1021/ja508629m | J. Am. Chem. Soc. 2014, 136, 15394−15402

Table 1. Calculated and Experimental CO Vibrational Frequencies for the H-cluster Model Intermediates Described in Figure 4

		CO Vibrational Frequencies (cm^{-1})	
Model	169 Group	DFT	Experimental[b,c]
1a	-SH	1841, 1949, 1989	1802, 1940, 1964
2a		1905, 1991, 2011	*not observed*
3a		1879, 1972, 1992	1872, 1971, 1990
4a		1862, 1951, 1964	1861, 1961, 1979
5a		1803, 1891, 1904	1792, 1891, 1915
1b	-OH	1831, 1948, 1995	1798, 1936, 1969
2b		1902, 1992, 2012	*not observed*
3b		1878, 1971, 1992	1874, 1967, 1987
4b		1862, 1951, 1965	1860, 1960, 1977
5b		ND[a]	1770, 1896, 1914

[a]ND = not determined. [b]The ν_{CO} assignments for WT (Cys 169) CrHydA1 are shown in Figure S8 (Supporting Information).[15] [c]Experimental ν_{CO} peaks of Cys169Ser are matched to DFT models **3b** and **4b** on the basis of alignment with WT spectra (Figure S8, Supporting Information).

conclusion is further supported by the EPR spectra, for which similar rhombic signals are observed in both Cys169Ser and WT under reduction (vide infra). Multiple theoretical studies have predicted formation of a $[2Fe]_H$ intermediate with $Fe^{II}Fe^{II}$ oxidation states upon H_2 binding and activation at the H-cluster.[19,49,50] Experimental evidence from X-ray absorption studies on CrHydA1 also indicated a slight oxidation of $[2Fe]_H$ upon H_2 binding by H_{ox},[57] consistent with the transition of $[2Fe]_H$ from $Fe^{II}Fe^{I}$ to $Fe^{II}Fe^{II}$.

Disruption of PT in Cys169Ser Causes a Shift in the Steady-State Equilibria of H-cluster Redox States. The strong bias for CrHydA1 Cys169Ser to equilibrate into a $[4Fe\text{-}4S]^{+}\text{-}Fe^{II}Fe^{II}$ oxidation state is again consistent with the Cys-to-Ser substitution disrupting fast PT during the catalytic cycle of the H-cluster. The ν_{CO} peaks observed in the reduced WT CrHydA1 that occur at 1882, 1891, 1919, 1920, and 1954 cm^{-1} are significantly weaker in the FTIR of reduced Cys169Ser. Our initial assignments of WT CrHydA1 EPR signals observed under NaDT reduction (rhombic 2.08) and H_2 reduction (broad 2.3−2.07) were H_{sred} or $[4Fe\text{-}4S]_H^{+}\text{-}Fe^{I}Fe^{I}$ and $[4Fe\text{-}4S]_H^{+}\text{-}Fe^{II}Fe^{II}$ state, respectively.[15] A more comprehensive analysis that considers the results presented here for Cys169Ser suggests the rhombic 2.07/2.08 signals better correlate to a $[4Fe\text{-}4S]_H^{+}\text{-}Fe^{II}Fe^{II}$ assignment. The contribution of the broad signal is strongest in the WT EPR spectrum when the 1883, 1891, 1916, and 1933 cm^{-1} ν_{CO} peaks dominate the FTIR spectrum,[15] suggesting these might be assigned to a $[4Fe\text{-}4S]_H^{+}\text{-}Fe^{I}Fe^{I}$ H-cluster. Likewise, the rhombic 2.08 signal in WT CrHydA1 correlated best with the occurrence of 1861, 1961, and 1979 cm^{-1} ν_{CO} peaks,[15] which matches with the rhombic 2.07 signal and higher energy ν_{CO} peaks of Cys169Ser (Figure 2). By comparison, the H_{sred} state of WT CrHydA1 described by Adamaska et al.[16] as $[4Fe\text{-}4S]_H^{+}\text{-}Fe^{I}Fe^{I}$ was formed under reduction by NaDT and 100% H_2 with ν_{CO} peaks at 1882, 1919, and 1954 cm^{-1} and a rhombic EPR signal (g = 2.076, 1.943, 1.868; Table S2, Supporting Information). Although the catalytic relevance of H_{sred} has recently been questioned,[58] these studies indicate that formation of H_{red} and H_{sred} requires functional PT and that reduction of the $[2Fe]_H$ subcluster to the $Fe^{I}Fe^{I}$ level is accomplished via a PCET mechanism.

Modification of the PT pathway and the subsequent prevention of electronic transitions at the H-cluster may also explain accumulation of a $[4Fe\text{-}4S]H^{+}$ subcluster signal in the EPR spectrum of reduced Cys169Ser. Intramolecular electron transfer between the $[4Fe\text{-}4S]_H$ and $[2Fe]_H$ subclusters is facilitated by strong spin coupling exchange through the bridging Cys thiolate.[37,38,52,59−61] This coupling may be disrupted when PT and ET steps are decoupled in Cys169Ser, further demonstrating that the electronic properties of the H-cluster are tightly coupled to its surrounding protein framework.[28,60,62−66]

In addition, the substitution of a more electronegative group such as −OH for −SH just 3.5 Å away from the bridgehead amine could alter the H-cluster interaction and cause changes to the electronic distribution. Model studies on $[2Fe]_H$ compounds show that electron delocalization extends into the adt ligand, suggesting that nearby changes such as H bonding or differences in protonation state of the bridgehead amine could result in different H-cluster properties.[67] The latter observation is consistent with the calculations here, which give different ν_{CO} frequencies for H-cluster states where the only difference is the protonation state of the bridgehead (Figure 4 and Table 1). Interestingly, the upward ν_{CO} shifts observed in this study compare nicely to FTIR of a NaDT reduced CrHydA1 that was reconstituted with a synthetic $[2Fe]_H$ mimic containing an O atom in the form of pdt in place of N at the bridgehead position.[13]

Spectroscopic Properties of CO Treated Cys169Ser. CO is known to inhibit [FeFe]-hydrogenase catalytic activity by binding reversibly to the terminal site on Fe_d of the oxidized $[2Fe]_H$ subcluster,[68] which results in distinctive H_{ox}-CO signals in both EPR[39,69,70] and FTIR spectra.[36,71] Thus, the requirement for an open site on Fe_d for exogenous CO binding and the unique spectral signatures provide a means to probe the coordination sphere and occupancy of Fe_d.

The interaction of CO with Cys169Ser was explored by exposing samples to 100% CO gas followed by EPR and IR spectroscopy. In contrast to WT CrHydA1, incubation of either the as-isolated or NaDT reduced Cys169Ser with 100% CO did not produce a characteristic H_{ox}-CO EPR axial signal (data not shown).[15,28,72] By comparison, treatment of the auto-oxidized Cys169Ser with CO (Figure 5A versus 5B) yielded an axial 2.05 signal (g = 2.047, 2.005, 2.007) with properties similar to that of the H_{ox}-CO signal of WT CrHydA1 (Table S2, Supporting Information).[15,28,72] This signal coincided with the complete replacement (or attenuation) of the rhombic 2.1 H_{ox} signal (Figure 5C). However, the intensity of the rhombic 2.06 signal present in the auto-oxidized EPR spectrum remained unchanged after CO exposure, indicating that this H-cluster species does not readily react with CO (Figure 5C). The observations that the H_{ox} state in Cys169Ser occurs only after prolonged auto-oxidation, that CO requires an open coordination site on Fe_d to induce formation of H_{ox}-CO,[68,73] and that the state that gives rise to the rhombic 2.06 signal does not readily react with CO are consistent with Cys169Ser equilibrating into a reduced state that harbors a terminally bound H-species.

dx.doi.org/10.1021/ja508629m | J. Am. Chem. Soc. 2014, 136, 15394−15402

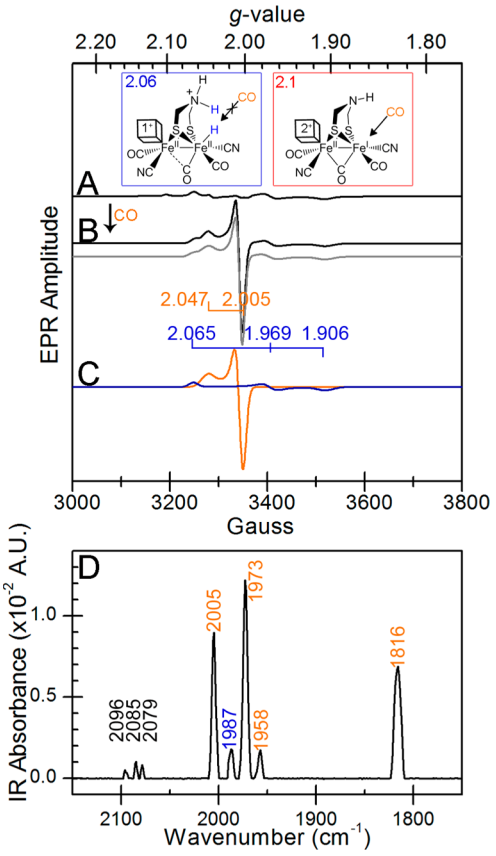

Figure 5. EPR (top panel) and FTIR (bottom panel) of auto-oxidized Cys169Ser treated with 100% CO: (A) auto-oxidized sample; (B) auto-oxidized sample sparged with CO (black) and simulation (gray); (C) individual simulations of the rhombic 2.06 (blue, 45%) and axial 2.05 (red, 55%) components of the overall signal; (D) auto-oxidized sample sparged with CO. Peak assignments in orange designate the ν_{CO} peaks assigned to the $H_{ox\text{-}CO}$ state and correlate with the axial 2.05 EPR signal. The peak in blue correlates with the residual rhombic 2.06 EPR signal. The sample concentration was 12 mg/mL, and the EPR temperature was 23 K; other spectrometer settings are as in the Figure 2 caption.

Likewise, the FTIR spectrum of Cys169Ser sample also showed the strongest H_{ox}-CO signal after auto-oxidization and CO treatment. The H_{ox}-CO spectrum of Cys169Ser was similar to that of WT, showing an upshift of μ-CO from 1802 to 1816 cm^{-1}, with an additional ν_{CO} peak at 2005 cm^{-1} consistent with addition of a terminally bound, exogenous CO (Figure 5D). For WT CrHydA1, binding of an exogenous CO to the terminal site of $[2Fe]_H$ gives rise to a peak at 2013 cm^{-1}. The 7 cm^{-1} difference between this ν_{CO} peak in Cys169Ser versus WT may arise from slight differences in coordination of other CO and CN^- ligands or H bonding and charge distribution around the H cluster.

Accumulation of a Reduced Intermediate with a Hydrogen Species Bound to $[2Fe]_H$ of Cys169Ser. The observation that Cys169Ser forms a reduced state that does not easily react with CO (Figure 5) suggests that the CO binding site, located at the open coordination site of Fe_d in $[2Fe]_H$,[68] is occupied by another terminal ligand. Since H_2 formation and oxidation is a two-proton process, an intermediate such as $[4Fe\text{-}4S]_H^+$-$Fe^{II}Fe^{II}$-H^- might accumulate, which is consistent with EPR/FTIR spectra and the observed isotope-sensitive ν_{CO} modes. Similar spectral features are observed in reduced WT CrHydA1, but at lower intensities in comparison to those for Cys169Ser. These differences can also be explained by a shift in the equilibrium of reduced states due to a modification of PT (kinetic effect), shifts in the polarity of residue 169 (SH → OH), and/or a shift in the midpoint potential of reduced states (thermodynamic effect).

The enrichment of an H_2-derived ligand bound at Fe_d fits the model of catalysis, for which protons are shuttled between the enzyme surface and catalytic site with the terminal step of the primary PT pathway being proton exchange between Cys169 and adt. Cys-to-Ser substitution is likely to slow this step and indirectly limit the exchange of protons between Fe_d of $[2Fe]_H$ and adt, possibly by disrupting the H-bonding network of the pathway.[31] While the Cys residue belongs to the primary PT pathway, several secondary PT networks have been identified[27] that perhaps assume the function of PT in Cys169Ser. This may explain the observations in this study that, although Cys169Ser has much lower catalytic activity, it still exhibits spectral properties of H-cluster electronic and structural transitions.

CONCLUSIONS

Using EPR and FTIR spectroscopy in conjunction with DFT calculations, we have provided evidence that disruption of the primary PT pathway by the Cys169 → Ser substitution in CrHydA1 substantially reduces catalytic activity and alters steady-state equilibration of the H-cluster among catalytic states. We hypothesize that this effect arises from decoupling of PT and ET steps but may also include contributions from changes in H-cluster midpoint potentials with Cys → Ser exchange. We demonstrated that, under reduction, Cys169Ser was biased toward H-cluster states consisting of an $S = 1/2$, $[4Fe\text{-}4S]_H^+$ subcluster, signifying the importance of intramolecular ET to catalysis by [FeFe]-hydrogenase. Likewise, the FTIR spectra and DFT calculations showed that the $[2Fe]_H$ subcluster of Cys169Ser was biased more strongly toward a $Fe^{II}Fe^{II}$ redox state. The fact that one of these diferrous states (rhombic 2.06) was unreactive with CO and showed an H → D isotope-sensitive μ-CO is consistent with the presence of an exchangeable, terminal H-species trans to μ-CO. The properties of these $[4Fe\text{-}4S]_H^+$-$Fe^{II}Fe^{II}$ H-cluster states agree well with the activation model of H_2 by the H-cluster. Indeed, DFT calculations on the model used in this work show that activation of H_2 in a $[4Fe\text{-}4S]^{2+}$-$Fe^{II}Fe^{II}$ H-cluster is slightly exothermic by −2 kcal/mol, whereas activation on the corresponding $[4Fe\text{-}4S]^{2+}$-$Fe^{II}Fe^{I}$ cluster is endothermic by +5 kcal/mol. A diferrous activation state was also proposed earlier by Fan and Hall[19] and supported by recent results on an H-cluster model where heterolytic cleavage of H_2 by the $[2Fe]_H$ subsite was stimulated by initial oxidation to the diferrous state by a covalently attached ferrocene.[8]

ASSOCIATED CONTENT

Supporting Information

Table, figures, and text describing the computational model of the H-cluster, EPR signals, temperature profiles, and power saturation data, FTIR isotope spectra, Cys298Ser CaI spectrum, difference spectra of WT and Cys169Ser CrHydA1 treated with H_2, and NaDT reduced CrHydA1 spectrum, and a detailed materials and methods section. This material is available free of charge via the Internet at http://pubs.acs.org.

AUTHOR INFORMATION

Corresponding Author

*E-mail for P.W.K.: paul.king@nrel.gov.

Notes

The authors declare no competing financial interest.

ACKNOWLEDGMENTS

D.W.M, M.W.R., and P.W.K. gratefully acknowledge funding support from the U.S. Department of Energy, Office of Science, Basic Energy Sciences, Division of Chemical Sciences, Geosciences, and Biosciences, and the support of the U.S. Department of Energy under Contract No. DE-AC36-08-GO28308 with the National Renewable Energy Laboratory for the hydrogenase purification, biochemical, and spectroscopy studies. M.B. and C.G. acknowledge the University of Milano-Bicocca (FAR 2013) for support of studies on H-cluster models and DFT calculations. E.K. and J.W.P. thank the Air Force Office of Scientific Research (grant FA-9550-11-1-0218) for funding support.

REFERENCES

(1) Lee, H. S.; Vermaas, W. F.; Rittmann, B. E. *Trends Biotechnol.* **2010**, *28*, 262.
(2) Sakurai, H.; Masukawa, H.; Kitashima, M.; Inoue, K. *J. Photochem. Photobiol., C* **2013**, *17*, 1.
(3) Vincent, K. A.; Parkin, A.; Armstrong, F. A. *Chem. Rev.* **2007**, *107*, 4366.
(4) Chenevier, P.; Mugherli, L.; Darbe, S.; Darchy, L.; DiManno, S.; Tran, P. D.; Valentino, F.; Iannello, M.; Volbeda, A.; Cavazza, C. *C. R. Chim.* **2013**, *16*, 491.
(5) Gloaguen, F.; Rauchfuss, T. B. *Chem. Soc. Rev.* **2009**, *38*, 100.
(6) DuBois, M. R.; DuBois, D. L. *Chem. Soc. Rev.* **2009**, *38*, 62.
(7) Tard, C.; Liu, X.; Ibrahim, S. K.; Bruschi, M.; De Gioia, L.; Davies, S. C.; Yang, X.; Wang, L.-S.; Sawers, G.; Pickett, C. J. *Nature* **2005**, *433*, 610.
(8) Camara, J. M.; Rauchfuss, T. B. *Nat. Chem.* **2012**, *4*, 26.
(9) Hsieh, C. H.; Ding, S.; Erdem, O. F.; Crouthers, D. J.; Liu, T.; McCrory, C. C.; Lubitz, W.; Popescu, C. V.; Reibenspies, J. H.; Hall, M. B.; Darensbourg, M. Y. *Nat. Commun.* **2014**, *5*, 3684.
(10) Nicolet, Y.; Piras, C.; Legrand, P.; Hatchikian, C. E.; Fontecilla-Camps, J. C. *Struct. Fold. Des.* **1999**, *7*, 13.
(11) Peters, J. W.; Lanzilotta, W. N.; Lemon, B. J.; Seefeldt, L. C. *Science* **1998**, *282*, 1853.
(12) Silakov, A.; Wenk, B.; Reijerse, E.; Lubitz, W. *Phys. Chem. Chem. Phys.* **2009**, *11*, 6592.
(13) Berggren, G.; Adamska, A.; Lambertz, C.; Simmons, T.; Esselborn, J.; Atta, M.; Gambarelli, S.; Mouesca, J.-M.; Reijerse, E.; Lubitz, W. *Nature* **2013**, *499*, 66.
(14) Lambertz, C.; Chernev, P.; Klingan, K.; Leidel, N.; Sigfridsson, K. G.; Happe, T.; Haumann, M. *Chem. Sci.* **2014**, *5*, 1187.
(15) Mulder, D. W.; Ratzloff, M. W.; Shepard, E. M.; Byer, A. S.; Noone, S. M.; Peters, J. W.; Broderick, J. B.; King, P. W. *J. Am. Chem. Soc.* **2013**, *135*, 6921.
(16) Adamska, A.; Silakov, A.; Lambertz, C.; Rudiger, O.; Happe, T.; Reijerse, E.; Lubitz, W. *Angew. Chem., Int. Ed.* **2012**, *51*, 11458.
(17) Adamska-Venkatesh, A.; Krawietz, D.; Siebel, J.; Weber, K.; Happe, T.; Reijerse, E.; Lubitz, W. *J. Am. Chem. Soc.* **2014**, *136*, 11339.
(18) Florin, L.; Tsokoglou, A.; Happe, T. *J. Biol. Chem.* **2001**, *276*, 6125.
(19) Fan, H. J.; Hall, M. B. *J. Am. Chem. Soc.* **2001**, *123*, 3828.
(20) Nicolet, Y.; de Lacey, A. L.; Vernede, X.; Fernandez, V. M.; Hatchikian, E. C.; Fontecilla-Camps, J. C. *J. Am. Chem. Soc.* **2001**, *123*, 1596.
(21) Finkelmann, A. R.; Stiebritz, M. T.; Reiher, M. *Chem. Sci.* **2014**, *5*, 215.
(22) Siegbahn, P. E.; Tye, J. W.; Hall, M. B. *Chem. Rev.* **2007**, *107*, 4414.
(23) Fourmond, V.; Greco, C.; Sybirna, K.; Baffert, C.; Wang, P.-H.; Ezanno, P.; Montefiori, M.; Bruschi, M.; Meynial-Salles, I.; Soucaille, P. *Nat. Chem.* **2014**, *6*, 336.
(24) Dutta, A.; Lense, S.; Hou, J.; Engelhard, M. H.; Roberts, J. A.; Shaw, W. J. *J. Am. Chem. Soc.* **2013**, *135*, 18490.
(25) Hong, G.; Cornish, A.; Hegg, E.; Pachter, R. *Biochim. Biophys. Acta, Bioenerg.* **2011**, *1807*, 510.
(26) Fontecilla-Camps, J. C.; Volbeda, A.; Cavazza, C.; Nicolet, Y. *Chem. Rev.* **2007**, *107*, 4273.
(27) Cornish, A. J.; Gärtner, K.; Yang, H.; Peters, J. W.; Hegg, E. L. *J. Biol. Chem.* **2011**, *286*, 38341.
(28) Knörzer, P.; Silakov, A.; Foster, C. E.; Armstrong, F. A.; Lubitz, W.; Happe, T. *J. Biol. Chem.* **2012**, *287*, 1489.
(29) Lautier, T.; Ezanno, P.; Baffert, C.; Fourmond, V.; Cournac, L.; Fontecilla-Camps, J. C.; Soucaille, P.; Bertrand, P.; Meynial-Salles, I.; Léger, C. *Faraday Discuss.* **2011**, *148*, 385.
(30) Morra, S.; Giraudo, A.; Di Nardo, G.; King, P. W.; Gilardi, G.; Valetti, F. *PloS one* **2012**, *7*, e48400.
(31) Ginovska-Pangovska, B.; Ho, M.-H.; Linehan, J. C.; Cheng, Y.; Dupuis, M.; Raugei, S.; Shaw, W. J. *Biochim. Biophys. Acta, Bioenerg.* **2014**, *1837*, 131.
(32) Long, H.; King, P. W.; Chang, C. H. *J. Phys. Chem. B* **2014**, *118*, 890.
(33) Mulder, D. W.; Shepard, E. M.; Meuser, J. E.; Joshi, N.; King, P. W.; Posewitz, M. C.; Broderick, J. B.; Peters, J. W. *Structure* **2011**, *19*, 1038.
(34) Patil, D. S.; Moura, J. J. G.; He, S. H.; Teixeira, M.; Prickril, B. C.; Dervartanian, D. V.; Peck, H. D.; Legall, J.; Huynh, B. H. *J. Biol. Chem.* **1988**, *263*, 18732.
(35) Pierik, A. J.; Hagen, W. R.; Redeker, J. S.; Wolbert, R. B.; Boersma, M.; Verhagen, M. F.; Grande, H. J.; Veeger, C.; Mutsaers, P. H.; Sands, R. H.; Dunham, W. R. *Eur. J. Biochem.* **1992**, *209*, 63.
(36) Pierik, A. J.; Hulstein, M.; Hagen, W. R.; Albracht, S. P. *Eur. J. Biochem.* **1998**, *258*, 572.
(37) Popescu, C. V.; Münck, E. *J. Am. Chem. Soc.* **1999**, *121*, 7877.
(38) Pereira, A. S.; Tavares, P.; Moura, I.; Moura, J. J. G.; Huynh, B. H. *J. Am. Chem. Soc.* **2001**, *123*, 2771.
(39) Albracht, S. P. J.; Roseboom, W.; Hatchikian, E. C. *J. Biol. Inorg. Chem.* **2006**, *11*, 88.
(40) Roseboom, W.; De Lacey, A. L.; Fernandez, V. M.; Hatchikian, E. C.; Albracht, S. P. J. *J. Biol. Inorg. Chem.* **2006**, *11*, 102.
(41) Silakov, A.; Kamp, C.; Reijerse, E.; Happe, T.; Lubitz, W. *Biochemistry* **2009**, *48*, 7780.
(42) King, P. W.; Posewitz, M. C.; Ghirardi, M. L.; Seibert, M. *J. Bacteriol.* **2006**, *188*, 2163.
(43) Yacoby, I.; Tegler, L. T.; Pochekailov, S.; Zhang, S.; King, P. W. *PloS One* **2012**, *7*, e35886.
(44) Ahlrichs, R.; Bär, M.; Häser, M.; Horn, H.; Kölmel, C. *Chem. Phys. Lett.* **1989**, *162*, 165.
(45) Becke, A. D. *Phys. Rev. A* **1988**, *38*, 3098.
(46) Perdew, J. P. *Phys. Rev. B* **1986**, *33*, 8822.
(47) Eichkorn, K.; Treutler, O.; Öhm, H.; Häser, M.; Ahlrichs, R. *Chem. Phys. Lett.* **1995**, *240*, 283.
(48) Schäfer, A.; Huber, C.; Ahlrichs, R. *J. Chem. Phys.* **1994**, *100*, 5829.
(49) Yu, L.; Greco, C.; Bruschi, M.; Ryde, U.; De Gioia, L.; Reiher, M. *Inorg. Chem.* **2011**, *50*, 3888.
(50) Liu, Z.-P.; Hu, P. *J. Am. Chem. Soc.* **2002**, *124*, 5175.
(51) Tye, J. W.; Darensbourg, M. Y.; Hall, M. B. *Inorg. Chem.* **2008**, *47*, 2380.
(52) Fiedler, A. T.; Brunold, T. C. *Inorg. Chem.* **2005**, *44*, 9322.
(53) Kaesz, H. D.; Saillant, R.-B. *Chem. Rev.* **1972**, *72*, 231.
(54) van der Vlugt, J. I.; Rauchfuss, T. B.; Whaley, C. M.; Wilson, S. R. *J. Am. Chem. Soc.* **2005**, *127*, 16012.
(55) Meng, J.; Smirnova, T. I.; Song, X.; Moore, A.; Ren, X.; Kelley, S.; Park, S.; Tilotta, D. *RSC Adv.* **2014**, *4*, 29840.
(56) Vaska, L. *J. Am. Chem. Soc.* **1966**, *88*, 4100.

(57) Stripp, S.; Sanganas, O.; Happe, T.; Haumann, M. *Biochemistry* **2009**, *48*, 5042.
(58) Hajj, V.; Baffert, C.; Sybirna, K.; Meynial-Salles, I.; Soucaille, P.; Bottin, H.; Fourmond, V.; Léger, C. *Energy Environ. Sci.* **2014**, *7*, 715.
(59) Silakov, A.; Reijerse, E. J.; Albracht, S. P. J.; Hatchikian, E. C.; Lubitz, W. *J. Am. Chem. Soc.* **2007**, *129*, 11447.
(60) Greco, C.; Bruschi, M.; Heimdal, J.; Fantucci, P.; De Gioia, L.; Ryde, U. *Inorg. Chem.* **2007**, *46*, 7256.
(61) Schwab, D. E.; Tard, C.; Brecht, E.; Peters, J. W.; Pickett, C. J.; Szilagyi, R. K. *Chem. Commun.* **2006**, 3696.
(62) Giles, L. J.; Grigoropoulos, A.; Szilagyi, R. K. *Eur. J. Inorg. Chem.* **2011**, *2011*, 2677.
(63) Miyake, T.; Bruschi, M.; Cosentino, U.; Baffert, C.; Fourmond, V.; Léger, C.; Moro, G.; De Gioia, L.; Greco, C. *J. Biol. Inorg. Chem.* **2013**, *18*, 693.
(64) Bruschi, M.; Greco, C.; Kaukonen, M.; Fantucci, P.; Ryde, U.; De Gioia, L. *Angew. Chem., Int. Ed.* **2009**, *48*, 3503.
(65) Winkler, M.; Esselborn, J.; Happe, T. *Biochim. Biophys. Acta, Bioenerg.* **2013**, *1827*, 974.
(66) Trohalaki, S.; Pachter, R. *Int. J. Hydrogen Energy* **2010**, *35*, 5318.
(67) Erdem, Ö. F.; Stein, M.; Kaur-Ghumaan, S.; Reijerse, E. J.; Ott, S.; Lubitz, W. *Chem. Eur. J.* **2013**, *19*, 14566.
(68) Lemon, B. J.; Peters, J. W. *Biochemistry* **1999**, *38*, 12969.
(69) Adams, M. *J. Biol. Chem.* **1987**, *262*, 15054.
(70) Erbes, D. L.; Burris, R.; Orme-Johnson, W. *Proc. Natl. Acad. Sci. U.S.A.* **1975**, *72*, 4795.
(71) Chen, Z.; Lemon, B. J.; Huang, S.; Swartz, D. J.; Peters, J. W.; Bagley, K. A. *Biochemistry* **2002**, *41*, 2036.
(72) Kamp, C.; Silakov, A.; Winkler, M.; Reijerse, E. J.; Lubitz, W.; Happe, T. *Biochim. Biophys. Acta, Bioenerg.* **2008**, *1777*, 410.
(73) Bennett, B.; Lemon, B. J.; Peters, J. W. *Biochemistry* **2000**, *39*, 7455.